Materials Research Letters

ISSN: (Print) (Online) Journal homepage: https://www.tandfonline.com/loi/tmrl20

Effective and back stresses evolution upon cycling a high-entropy alloy

Kaiju Lu, Ankur Chauhan, Fabian Knöpfle & Jarir Aktaa

To cite this article: Kaiju Lu, Ankur Chauhan, Fabian Knöpfle & Jarir Aktaa (2022) Effective and back stresses evolution upon cycling a high-entropy alloy, Materials Research Letters, 10:6, 369-376, DOI: 10.1080/21663831.2022.2054667

To link to this article: https://doi.org/10.1080/21663831.2022.2054667

Published online: 23 Mar 2022.

MATER. RES. LETT.
2022, VOL. 10, NO. 6, 369–376
https://doi.org/10.1080/21663831.2022.2054667

MATERIALS RESEARCH LETTERS
Taylor & Francis
Taylor & Francis Group

ORIGINAL REPORTS

Effective and back stresses evolution upon cycling a high-entropy alloy

Kaiju Lu [a], Ankur Chauhan [a,b], Fabian Knöpfle[a] and Jarir Aktaa[a]

[a]Institute for Applied Materials, Karlsruhe Institute of Technology (KIT), Eggenstein-Leopoldshafen, Germany; [b]Department of Materials Engineering, Indian Institute of Science, Bengaluru, India

ABSTRACT

We report on the effective and back stresses evolution of a CoCrFeMnNi high-entropy alloy (HEA) by partitioning its cyclic hysteresis loops. It was found that the cyclic stress response of the HEA predominantly originates from the back stress evolution. Back stress also increases significantly with increasing strain amplitude and reducing grain size. However, the change of effective stress is rather insignificant with altering cycle number, strain amplitude and grain size. This indicates that the effective stress is determined mainly by the lattice friction. Further comparisons to an austenitic steel and a medium-entropy alloy identified the origins of their peculiar cyclic strength.

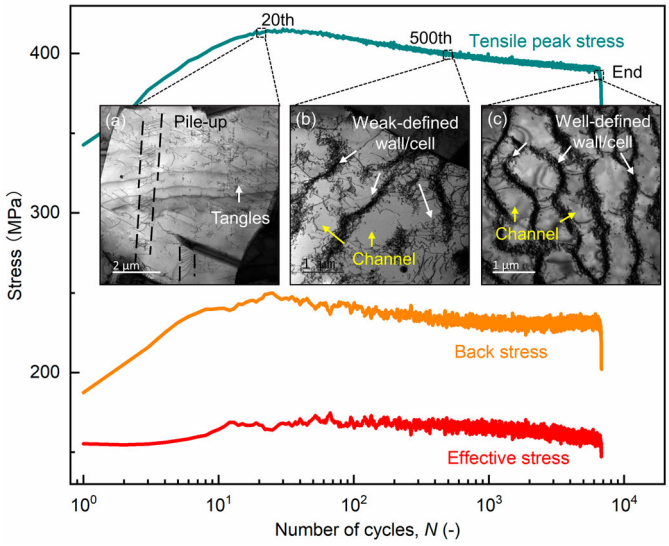

ARTICLE HISTORY
Received 24 December 2021

KEYWORDS
High-entropy alloy; fatigue; effective stress; back stress

IMPACT STATEMENT

The effective stress and back stress upon cycling a HEA are assessed, both of which are higher than a conventional FCC steel, contributing to the HEA's higher cyclic strength.

1. Introduction

Recently, considerable efforts have been put into understanding the low-cycle fatigue (LCF) behavior and microstructural evolution of high-entropy alloys (HEAs) [1–5]. For instance, the equiatomic face-centered cubic (FCC) CoCrFeMnNi HEA was reported to show higher lattice friction [6], comparable or even higher LCF resistance [1,7] compared to conventional FCC alloys. However, limited attention has been paid for interpreting the origin of HEAs' cyclic stress response and the types of obstacles to dislocation motion.

It is widely accepted that the total flow stress can be divided into two components, namely, effective stress and back stress [8–11]. The understanding of these stresses' evolution is essential to describe materials' constitutive behavior, such as dislocation slip behavior [10,12]. In detail, effective stress is required locally for a mobile dislocation to overcome short-range obstacles, such as

CONTACT Kaiju Lu kaiju.lu@hotmail.com; kaiju.lu@kit.edu Institute for Applied Materials, Karlsruhe Institute of Technology (KIT), Hermannvon-Helmholtz-Platz 1, 76344 Eggenstein-Leopoldshafen, Germany

This article has been corrected with minor changes. These changes do not impact the academic content of the article.

lattice friction and dislocations forest [11,13,14]. Back stress refers to long-range resistance stress from grain boundaries and dislocation substructures [14–16] and is often related to Bauschinger effect.

Many attempts have been made to determine the effective and back stresses of different conventional FCC materials [12,17–25] by different tests. Taking FCC 316 steel as an example, upon cycling, the effective stress remains constant during most of its fatigue life; and the back stress mainly defines its cyclic stress response [19]. For HEAs, in the only study using tension-compression tests rather than fully reversed fatigue tests, Bouaziz et al. [11] attributed high back stresses of CoCrFeMnNi HEA to the low probability of cross-slip. It is also essential to elucidate effective and back stresses evolution upon cyclic loading the HEA, which is anticipated to be unique from the results obtained in tension-compression tests [11].

Furthermore, our previous study [4] has suggested that CoCrFeMnNi shows higher cyclic strength than conventional 316L steel and manifests a transition from planar-slip to cross-slip (with increasing cycle number and strain amplitude). It is therefore of interest to clarify the origin of the HEA's higher cyclic strength and correlate it to the dislocation behavior. Likewise, the CoCrFeMnNi and its superior subset CoCrNi medium-entropy alloy (MEA) have been reported to exhibit different cyclic strength [2], with their effective and back stresses contribution yet to be compared.

Therefore, this work aims to provide fresh insights into the effective and back stresses evolution upon cycling the CoCrFeMnNi HEA (with emphasis on the influences of cycle number, strain amplitude and grain size), and further to compare them with a 316L steel as well as with CoCrNi MEA.

2. Experimental details

The investigated equiatomic CoCrFeMnNi was synthesized by arc melting followed by drop-casting, homogenization, and rotary-swaging. Cylindrical LCF specimens (with a gauge diameter of 2 mm and gauge length of 7.6 mm) were machined out from the rotary-swaged material. Prior to LCF tests, the specimens were recrystallized by annealing for 1 h at 800°C and 1000°C, respectively, to obtain different grain sizes of the alloy [$\sim 6 \pm 3\,\mu$m and $\sim 50 \pm 30\,\mu$m, referred to as fine-grained (FG) and coarse-grained (CG), respectively, hereafter]. Detailed microstructures of FG and CG materials can be found in Ref. [4].

Cyclic pull-to-push LCF tests were carried out in air at RT with an extensometer of 7 mm gauge length. All tests were conducted under a nominal strain rate of $3\times10^{-3}\,s^{-1}$ using a symmetrical triangular waveform (i.e. strain ratio R of -1) at different strain amplitudes (0.3%, 0.5% and 0.7%). To separate the contributions of effective and back stresses to the total flow stress, the hysteresis loops were analyzed using the Cottrell method (see Fig. A1) [14,15]. Notably, due to the current number of data points (i.e. 160) per half hysteresis loop, the calculated effective stress and back stresses have a scatter of $\sim(\pm10)$ MPa.

3. Results and discussion

3.1. Evolution with cycle number

Figure 1 presents the typical tensile peak, effective, and back stresses evolution with the number of cycles for the FG CoCrFeMnNi sample tested at a strain amplitude of 0.5%. As evident, the effective stress increases marginally at initial cycles and then remains in a near -steady state before failure (Figure 1). However, the back stress evolution almost replicates the general trend of the tensile peak stress, i.e. an initial increase (cyclic hardening) followed by a decrease (cyclic softening) and near-steady state until failure (Figure 1). Notably, the above trend of effective and back stresses is also applicable for other strain amplitudes (0.3% and 0.7%, see Figure 2) and CG material (Figure 3).

The above stresses evolution with cycle number can be linked to the previously reported dislocation structures at different stages that were revealed by transmission electron microscope (TEM) investigations [4]. In specific, with increasing cycle number (or stage), the dislocation structures have been reported to change from initial pile-up and tangles, to weak-defined wall/cell-like substructures, and finally to their well-defined versions [see insets (a–c) in Figure 1] [4].

Accordingly, for the effective stress, its initial marginal increase is related to the increased density of dislocation forest (i.e. in the form of tangles, see Figure 1(a) [4]). Afterwards, the nearly stabilized effective stress can be ascribed to the insignificant change in dislocation density during the near-steady stage.

For the back stress, at the *initial hardening* stage, the significant increase is linked to the dislocation pile-up against grain boundaries (see Figure 1(a) [4]). Moreover, at the initial stage, the increase in back stress is more pronounced than that in effective stress, indicating that dislocations pile-up is more prevalent than tangles. Thereafter, at the *softening* stage, the decrease in back stress can be ascribed to dislocations rearrangement into their weak-defined low-energy substructures (i.e. walls and cells separated by channels, e.g. see Figure 1(b) [4]). It is well accepted that the total back stress during

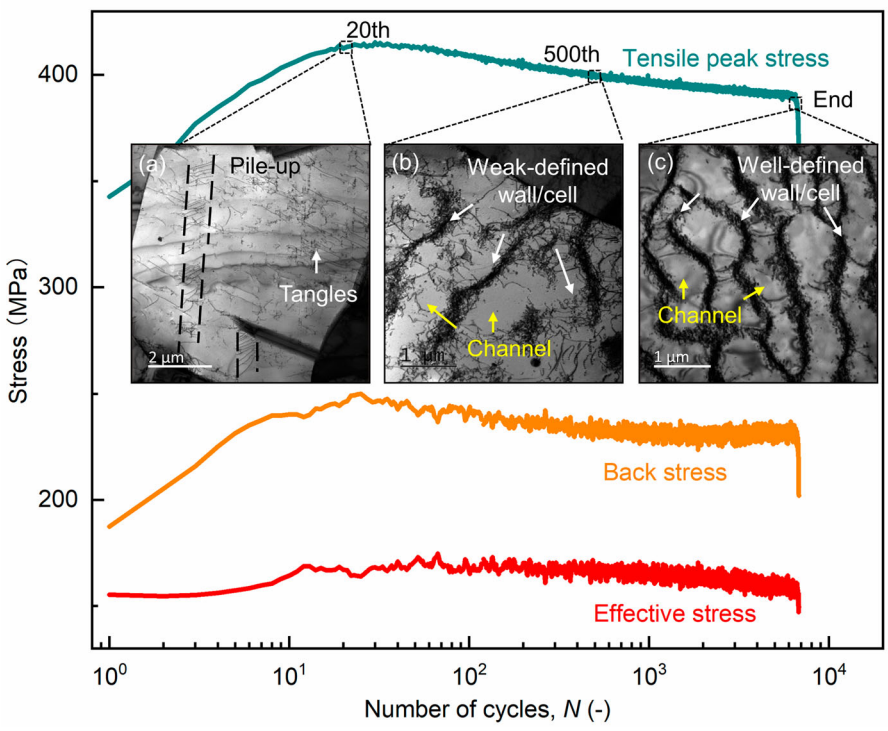

Figure 1. Typical tensile peak, effective and back stresses evolution with the number of cycles for a fine-grained (FG) CoCrFeMnNi specimen tested at RT and strain amplitude of 0.5%. The insets (a–c) are TEM micrographs acquired from specimens tested upto (a) 20, (b) 500, and (c) end-life cycles, representing cyclic hardening, softening and near-steady stages, respectively [4].

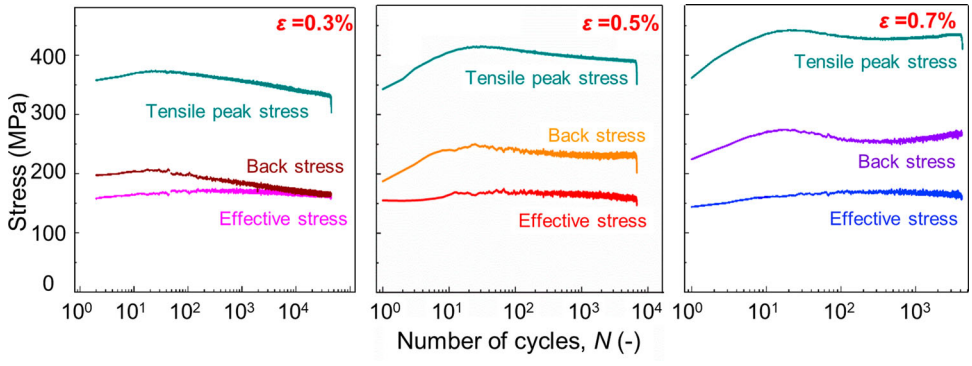

Figure 2. Tensile peak, effective and back stresses evolution with the number of cycles for FG CoCrFeMnNi specimens tested at RT and strain amplitude of 0.3%, 0.5%, and 0.7%.

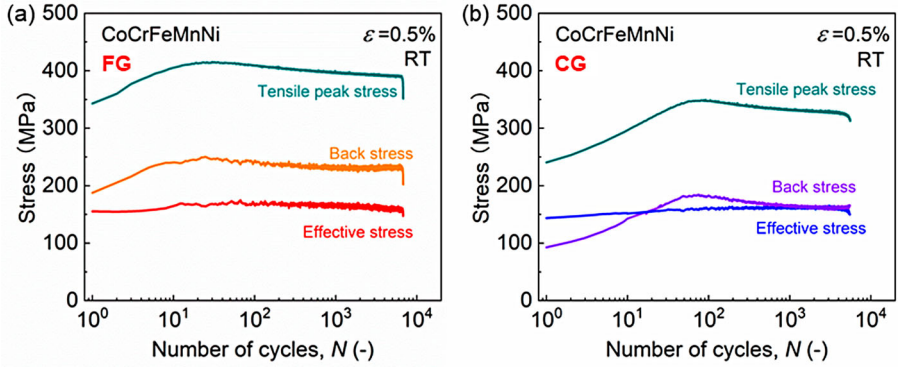

Figure 3. Tensile peak, effective and back stresses variation with the number of cycles for (a) fine-grained (FG) and (b) coarse-grained (CG) CoCrFeMnNi specimens tested at 0.5% strain amplitude.

straining polycrystals results from two incompatibility levels, i.e. intergranular (χ_{inter}) and intragranular (χ_{intra}) components [24]. On one hand, these substructures' formation reduces the χ_{inter} against grain boundaries. Specifically, their formation involves massive dislocations wavy/cross-slip induced annihilation, which lowers the number of dislocations in the pile-up; and thereby, reduces the χ_{inter}. On the other hand, their formation increases the χ_{intra}, due to dislocations piling up against walls and cells [26]. Taken together, the decrease in total back stress at this stage implies that the reduced χ_{inter} outweighs the increased χ_{intra}. Afterwards, at the *near-steady* stage, the change in back stresses is insignificant, which can be related to the inconsequential change in the configuration of dislocations, e.g. see Figure 1(b,c) [4]. This also suggests that a near-equilibrated status of the competition (between the increase of χ_{intra} and the decrease of χ_{inter}) is achieved. Therefore, in totality, the back stress evolution is correlated well with the dislocation structures evolution (i.e. from pile-up to low-energy substructures).

Overall, upon cycling CoCrFeMnNi, the change of cyclic stress (including hardening and softening) is mainly controlled by the back stress, which is irrespective of the applied strain amplitude. This observation is in general similar to that reported for FCC 316 steels [19,21–23].

3.2. Evolution with strain amplitude and grain size

Figure 2 shows the typical tensile peak, effective and back stresses evolution for FG CoCrFeMnNi specimens acquired a strain amplitude of 0.3%, 0.5%, and 0.7%. Clearly, with increasing applied strain amplitude, the back stress increases strikingly. However, despite the scatter that exists per cycle and strain amplitude, the increase in effective stress is insignificant.

Additionally, the percentage of back stress to stress amplitude was calculated from both FG and CG CoCrFeMnNi specimens at the saturated (e.g. half-life) cycles (see Table 1). As evident, the back stress represents a sizable portion of the stress amplitude ($\sim$40% to 60%), signifying the material's high kinematic hardening ability. Besides, the ratio of back stress increases with the strain amplitude (Table 1). This indicates that the strain hardening mostly originates from higher back stress.

To clarify the effect of grain size, Figure 3 shows the calculated stresses evolution of (a) FG and (b) CG CoCrFeMnNi tested at 0.5% strain amplitude. Apparently, by decreasing grain size, the increase of back stress is more significant than that of effective stress. For example, at strain amplitude 0.5% and half-life, with reducing grain size from CG to FG range, the saturated effective stress remains nearly constant ($\sim$160 MPa); whereas the saturated back stress increases by $\sim$70 MPa (Figure 3(a,b)). This result indicates that the higher grain boundary strengthening for FG CoCrFeMnNi contributes to its higher back stress, in comparison to the CG version. This is in line with the previous findings reported for nickel and 316L steel; i.e., in comparison to effective stress, back stress is more dependent on the grain size [18,27].

Table 1. The percentage of back stress to the stress amplitude at saturated (e.g. half-life) cycles of FG and CG CoCrFeMnNi specimens tested at different strain amplitudes.

	Strain amplitude		
Grain size	0.3%	0.5%	0.7%
FG	50.7%	58.8%	61.2%
CG	42.9%	49.9%	54.3%

Taken together, increasing strain amplitude and reducing grain size both lead to an increase in back stress. The as-expected significant increase in back stress herein can also be attributed to massive dislocations pile-up against grain boundaries and substructures, similar to that discussed in Section 3.1.

Meanwhile, the unexpected slight increase in effective stress (as a function of strain amplitude and/or cycle number) suggests that the effective stress for CoCrFeMnNi is determined more by lattice friction rather than forest hardening upon cycling. Similarly, the insignificant increase of effective stress was addressed in previous reports [22,23,28]. Further more, Hong and Laird [12,29] proposed that in copper alloys, the elastic interaction between dislocations and solute atoms is dominantly responsible for the evolution of effective stress.

Interestingly, upon tension-compression tests [11], the increase of effective stress is shown to be rather significant with increasing strain levels. For example, effective stress is estimated (by us from the tests in [11]) to increase from $\sim$127 to $\sim$161 MPa with increasing strain from 3% to 14%. This significant increase in effective stress for tension-compression tests could be ascribed to the increased cross slip probability and dislocations forest upon increasing strain levels.

3.3. In comparison to an austenitic steel

The above-presented effective and back stresses evolution with cycle number, strain amplitude and grain size for the FCC CoCrFeMnNi HEA is in general consistent with that of conventional austenitic steels [19–22]. This reflects that there are no new cyclic deformation mechanisms for the presently investigated HEA compared to austenitic steels.

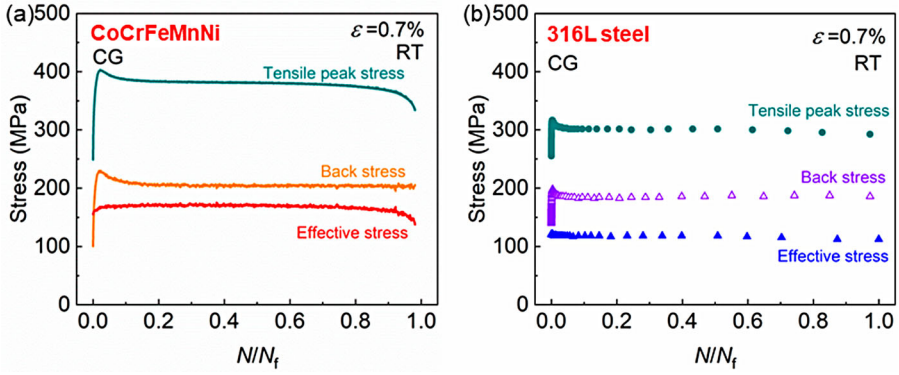

Figure 4. Tensile peak, effective and back stresses evolution with the *normalized* number of cycles (N/N_f) for (a) CoCrFeMnNi and (b) 316L steel [20] specimens tested at 0.7% strain amplitude and RT. Note that the CoCrFeMnNi and 316L steel have similar coarse grain (CG) size and insignificant texture.

Nevertheless, in comparison to similar grain-sized 316L austenitic steel, CoCrFeMnNi has been reported to show higher cyclic strength [4]. To further elucidate the origin of its higher cyclic strength, the effective and back stresses of the CG CoCrFeMnNi were compared to that of the CG 316L steel [20], see Figure 4.

Evidently, compared to 316L steel, CoCrFeMnNi exhibits both higher effective and back stresses under the same applied strain amplitude (0.7%). For example, the saturated effective and back stresses are ~50 MPa and ~20 MPa higher than that of the 316L steel. This indicates that, compared to 316L steel, the higher cyclic strength of CoCrFeMnNi arises from both higher lattice friction (or solid solution strengthening) and grain boundary strengthening, with the former one being the main contributor.

It is also of interest to note that deformation twins have been reported to occur in CG CoCrFeMnNi [4] and 316L steel [30] (both with a minor fraction). Deformation twins, having Σ3 grain boundaries, formation in a minor fraction could result in a slight increase of back stress for both materials.

3.4. In comparison to CoCrNi medium-entropy alloy

Though the above analysis is based on the LCF data for CoCrFeMnNi, it should be also applicable to a broader range of FCC HEAs and their MEA subsets. To verify this, the effective and back stresses evolution of fine-grained CoCrNi MEA tested at 0.7% strain amplitude were estimated and are shown in Figure 5(a).

As expected, similar to the CoCrFeMnNi, the tensile peak stress response of the CoCrNi MEA is also mainly dictated by the evolution of back stress upon LCF loading. It is well known that the strain-controlled LCF behavior is generally believed to be determined by the ductility of a material [31]. Therefore, the above stresses evolution is considered to also apply to other types of HEAs with high ductility, such as ductile body-centered cubic HEAs [32], in addition to FCC HEAs. Nevertheless, further efforts are needed for verification.

As a comparison, Figure 5(b) presents the stresses of FG CoCrFeMnNi tested at 0.7% strain amplitude. Likewise, the CoCrNi alloy shows both higher effective and back stresses than CoCrFeMnNi. For example, the saturated effective and back stresses of CoCrNi are ~40 MPa

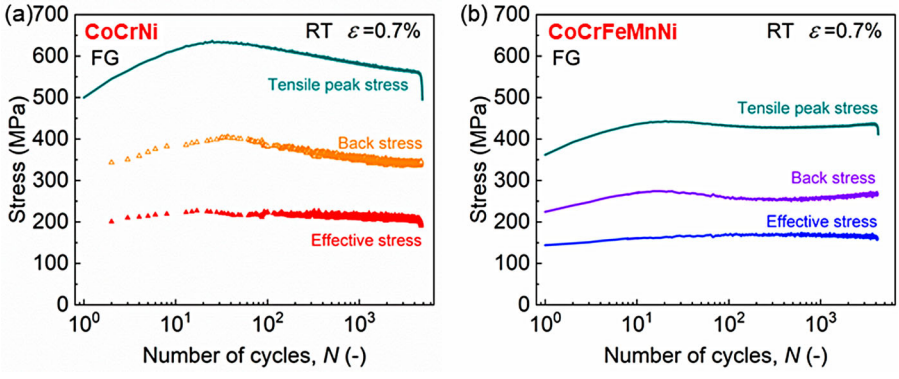

Figure 5. Tensile peak, effective and back stresses variation with the number of cycles for (a) CoCrNi and (b) CoCrFeMnNi specimens tested at 0.7% strain amplitude. Note that the CoCrNi and CoCrFeMnNi have similar fine grain (FG) size and insignificant texture.

and ~80 MPa higher than that of the CoCrFeMnNi. This suggests that the higher cyclic strength of CoCrNi results from the larger effective stress and even larger back stress than CoCrFeMnNi.

The higher effective stress in CoCrNi is ascribed to its larger solid solution hardening due to larger shear modulus, most likely coming from the high Cr content (higher mean atomic displacement) and the large volumetric mismatch among Cr (as the largest atom size and shear modulus in the system), Ni and Co (both comparably small) [33,34]. Whereas, the higher back stress is related to its higher grain boundary strengthening, which suggests higher Hall-Petch constant k of CoCrNi in comparison to CoCrFeMnNi.

For CoCrFeMnNi, the k value is well-accepted to be 494 MPa$\sqrt{\mu}$m [35]. However, for CoCrNi, there exists a large discrepancy regarding the k value, which is reported to be 265 MPa$\sqrt{\mu}$m [34] and 815 MPa$\sqrt{\mu}$m [36], respectively. The possible reasons for this discrepancy have been proposed to lie in their different preparation routes, grain size distribution, and impurity contamination levels [36]. Here, by using the same CoCrNi material to Ref. [36], the obtained higher back stress of CoCrNi suggests its larger k constant, as compared to CoCrFeMnNi. Hence, our finding supports the rationale reported in Ref. [36]. In addition, since the back stress exhibits a Hall-Petch type relation [18,27], the higher k value of a material can be taken as an indication of its higher back stress.

4. Summary

The key findings are summarized as below:

- At all investigated strain amplitudes, the cyclic stress response is dictated by the evolution of back stress, which is correlated well with dislocation structures transition (i.e. from pile-up to low-energy substructures).
- Unlike the remarkable increase of effective stress reported for tension-compression tests, effective stress does not change significantly with altering cycle number, strain amplitude and grain size upon cyclic loading. This suggests that effective stress is determined more by lattice friction than dislocation forest upon cycling.
- Besides, back stress increases significantly with increasing strain amplitude and reducing grain size. This indicates that both cyclic strain hardening and grain boundary hardening mostly derive from back stress.
- Compared to a 316L steel, CoCrFeMnNi HEA exhibits both higher effective stress and back stress, suggesting both higher solid solution strengthening and grain boundary strengthening in HEAs.
- The above analyses are also applicable for a wide range of HEAs and their MEA subsets (e.g. CoCrNi). In comparison to CoCrFeMnNi, the higher cyclic strength of CoCrNi stems from both higher effective stress and back stress.

Thus, this work provides the origin of the cyclic strength of a HEA and identifies the types of obstacles to dislocation motion upon cycling. Further quantitative analyses of the effective and back stresses are envisaged as future work.

Acknowledgements

The authors acknowledge Prof. Dr. M. Heilmaier, Dr. A. Kauffmann, and Dr. A. S. Tirunilai for providing the CoCrFeMnNi, Prof. Dr. G. Laplanche and Dr. M. Schneider for providing the CoCrNi, as well as Prof. Dr. J. Freudenberger for performing rotary-swaging. K. L. thanks Dr. D. Litvinov and Dr. M. Walter for their kind guidance in using the TEM and the fatigue testing machine. We also acknowledge support by the KIT-Publication Fund of the Karlsruhe Institute of Technology.

Disclosure statement

No potential conflict of interest was reported by the author(s).

ORCID

Kaiju Lu http://orcid.org/0000-0002-2819-5028
Ankur Chauhan http://orcid.org/0000-0002-6798-5882

References

[1] Shams SAA, Jang G, Won JW, et al. Low-cycle fatigue properties of CoCrFeMnNi high-entropy alloy compared with its conventional counterparts. Mater Sci Eng A. 2020;792:Article 139661. doi:10.1016/j.msea.2020.139661.
[2] Lu K, Chauhan A, Walter M, et al. Superior low-cycle fatigue properties of CoCrNi compared to CoCrFeMnNi. Scr Mater. 2021 Mar 15;194:Article 113667. doi:10.1016/j.scriptamat.2020.113667.
[3] Picak S, Wegener T, Sajadifar SV, et al. On the low cycle fatigue response of CoCrNiFeMn high entropy alloy with ultra-fine grain structure. Acta Mater. 2020 Dec 8:Article 116540. doi:10.1016/j.actamat.2020.116540.
[4] Lu K, Chauhan A, Tirunilai AS, et al. Deformation mechanisms of CoCrFeMnNi high-entropy alloy under low-cycle-fatigue loading. Acta Mater. 2021 Jun 16;215:Article 117089. doi:10.1016/j.actamat.2021.117089.
[5] Heczko M, Mazánová V, Slone CE, et al. Role of deformation twinning in fatigue of CrCoNi medium-entropy alloy at room temperature. Scr Mater. 2021;202. doi:10.1016/j.scriptamat.2021.113985.
[6] Lee S, Duarte MJ, Feuerbacher M, et al. Dislocation plasticity in FeCoCrMnNi high-entropy alloy: quantitative insights from in situ transmission electron microscopy

deformation. Mater Res Lett. 2020;8(6):216–224. doi:10.1080/21663831.2020.1741469.
[7] Lu K, Chauhan A, Litvinov D, et al. High-temperature low cycle fatigue behavior of an equiatomic CoCrFeMnNi high-entropy alloy. Mater Sci Eng A. 2020;791:Article 139781. doi:10.1016/j.msea.2020.139781.
[8] Ma E, Wu X. Tailoring heterogeneities in high-entropy alloys to promote strength-ductility synergy. Nat Commun. 2019 Dec 9;10(1):5623. PubMed PMID: 31819051; PubMed Central PMCID: PMCPMC6901531.
[9] Shi P, Ren W, Zheng T, et al. Enhanced strength-ductility synergy in ultrafine-grained eutectic high-entropy alloys by inheriting microstructural lamellae. Nat Commun. 2019 Jan 30;10(1):489. PubMed PMID: 30700708; PubMed Central PMCID: PMCPMC6353877.
[10] Basu I, De Hosson JTM. Strengthening mechanisms in high entropy alloys: fundamental issues. Scr Mater. 2020;187:148–156. doi:10.1016/j.scriptamat.2020.06.019.
[11] Bouaziz O, Moon J, Kim HS, et al. Isotropic and kinematic hardening of a high entropy alloy. Scr Mater. 2021;191:107–110. doi:10.1016/j.scriptamat.2020.09.022.
[12] Hong SI, Laird C. Cyclic deformation behavior of Cu-16at. %Al single crystals Part III: friction stress and back stress behavior. Mater Sci Eng A. 1990 Sep 1;128(2):155–169. doi:10.1016/0921-5093(90)90224-Q.
[13] Lomer W. A dislocation reaction in the face-centred cubic lattice. Lond Edinb Dublin Philos Mag J Sci. 1951;42(334):1327–1331.
[14] Cottrell AH, Dexter D. Dislocations and plastic flow in crystals. Am J Phys. 1954;22:242–243.
[15] Kuhlmann-Wilsdorf D, Laird C. Dislocation behavior in fatigue II. Friction stress and back stress as inferred from an analysis of hysteresis loops. Mater Sci Eng. 1979 Feb 1;37(2):111–120. doi:10.1016/0025-5416(79)90074-0.
[16] Mughrabi H. Deformation-induced long-range internal stresses and lattice plane misorientations and the role of geometrically necessary dislocations. Philos Mag. 2006;86(25-26):4037–4054. doi:10.1080/14786430500509054.
[17] Han D, Zhang YJ, Li XW. A crucial impact of short-range ordering on the cyclic deformation and damage behavior of face-centered cubic alloys: a case study on Cu-Mn alloys. Acta Mater. 2021;205. doi:10.1016/j.actamat.2020.116559.
[18] Haddou H, Risbet M, Marichal G, et al. The effects of grain size on the cyclic deformation behaviour of polycrystalline nickel. Mater Sci Eng A. 2004;379(1-2):102–111. doi:10.1016/j.msea.2003.12.069.
[19] Polák J, Fardoun F, Degallaix S. Effective and internal stresses in cyclic straining of 316 stainless steel. Mater Sci Eng A. 1996 Sep 15;215(1):104–112. doi:10.1016/0921-5093(96)10373-7.
[20] Pham MS, Holdsworth SR, Janssens KGF, et al. Cyclic deformation response of AISI 316L at room temperature: mechanical behaviour, microstructural evolution, physically-based evolutionary constitutive modelling. Int J Plast. 2013;47:143–164. doi:10.1016/j.ijplas.2013.01.017.
[21] Pham MS, Holdsworth SR. Evolution of relationships between dislocation microstructures and internal stresses of AISI 316L during cyclic loading at 293 K and 573 K (20 °C and 300 °C). Metall Mater Trans A. 2013;45(2):738–751. doi:10.1007/s11661-013-1981-7.
[22] Chang B, Zhang Z. Cyclic deformation behavior in a nitrogen-alloyed austenitic stainless steel in terms of the evolution of internal stress and microstructure. Mater Sci Eng A. 2012;556:625–632. doi:10.1016/j.msea.2012.07.037.
[23] Chang B, Zhang Z. Low cycle fatigue behavior of a high nitrogen austenitic stainless steel under uniaxial and non-proportional loadings based on the partition of hysteresis loops. Mater Sci Eng A. 2012;547:72–79. doi:10.1016/j.msea.2012.03.082.
[24] Feaugas X. On the origin of the tensile flow stress in the stainless steel AISI 316L at 300 K: back stress and effective stress. Acta Mater. 1999 Oct 8;47(13):3617–3632. doi:10.1016/S1359-6454(99)00222-0.
[25] Yang M, Pan Y, Yuan F, et al. Back stress strengthening and strain hardening in gradient structure. Mater Res Lett. 2016;4(3):145–151. doi:10.1080/21663831.2016.1153004.
[26] Mughrabi H. Dislocation wall and cell structures and long-range internal stresses in deformed metal crystals. Acta Metall. 1983 Sep 1;31(9):1367–1379. doi:10.1016/0001-6160(83)90007-X.
[27] Feaugas X, Haddou H. Grain-size effects on tensile behavior of nickel and AISI 316L stainless steel. Metall Mater Trans A. 2003 Oct 1;34(10):2329–2340. doi:10.1007/s11661-003-0296-5.
[28] Shao CW, Zhang P, Zhu YK, et al. Improvement of low-cycle fatigue resistance in TWIP steel by regulating the grain size and distribution. Acta Mater. 2017;134:128–142. doi:10.1016/j.actamat.2017.05.004.
[29] Hong SI, Laird C. Mechanisms of slip mode modification in F.C.C. solid solutions. Acta Metall Mater. 1990 Aug 1;38(8):1581–1594. doi:10.1016/0956-7151(90)90126-2.
[30] Gerland M, Mendez J, Violan P, et al. Evolution of dislocation structures and cyclic behaviour of a 316L-type austenitic stainless steel cycled in vacuo at room temperature. Mater Sci Eng A. 1989 Oct 1;118:83–95. doi:10.1016/0921-5093(89)90060-9.
[31] Suresh S. Fatigue of materials. Cambridge: Cambridge University Press; 1998.
[32] Pang J, Zhang H, Zhang L, et al. Ductile Ti1.5ZrNbAl0.3 refractory high entropy alloy with high specific strength. Mater Lett. 2021 May 1;290:Article 129428. doi:10.1016/j.matlet.2021.129428.
[33] Okamoto NL, Yuge K, Tanaka K, et al. Atomic displacement in the CrMnFeCoNi high-entropy alloy – a scaling factor to predict solid solution strengthening. AIP Adv. 2016;6(12):Article 125008. doi:10.1063/1.4971371.
[34] Yoshida S, Bhattacharjee T, Bai Y, et al. Friction stress and Hall-Petch relationship in CoCrNi equi-atomic medium entropy alloy processed by severe plastic deformation and subsequent annealing. Scr Mater. 2017;134:33–36. doi:10.1016/j.scriptamat.2017.02.042.
[35] Otto F, Dlouhý A, Somsen C, et al. The influences of temperature and microstructure on the tensile properties of a CoCrFeMnNi high-entropy alloy. Acta Mater. 2013;61:5743–5755.
[36] Schneider M, George EP, Manescau TJ, et al. Analysis of strengthening due to grain boundaries and annealing twin boundaries in the CrCoNi medium-entropy alloy. Int J Plast. 2019.

Appendix

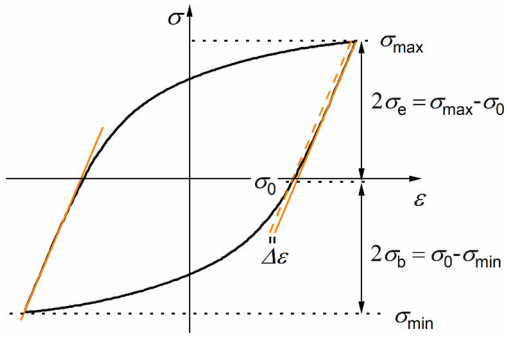

Figure A1. Schematic figure showing Cottrell's method of calculating effective stress (σ_e) and back stress (σ_b). Here, σ_0 is measured as the offset yield strength corresponding to an offset plastic strain ($\Delta\varepsilon$) of 0.1%.